This Accepted Manuscript has not been copyedited and formatted. The final version may differ from this version. A link to any extended data will be provided when the final version is posted online.

eNeuro

Research Article: New Research | Sensory and Motor Systems

Signature patterns for top-down and bottom-up information processing via cross-frequency coupling in macaque auditory cortex

Christian D. Márton[1,2], Makoto Fukushima[2,3,4], Corrie R. Camalier[2], Simon R. Schultz[1] and Bruno B. Averbeck[2]

[1]*Centre for Neurotechnology & Department of Bioengineering, Imperial College London, London, SW7 2AZ United Kingdom*

[2]*Laboratory of Neuropsychology, Section on Learning & Decision Making, NIMH/NIH, Bethesda, MD, USA*

[3]*RIKEN Brain Science Institute, Saitama, Japan*

[4]*Consumer Neuroscience, The Nielsen Company, Tokyo, Japan*

https://doi.org/10.1523/ENEURO.0467-18.2019

Received: 29 November 2018

Revised: 1 March 2019

Accepted: 5 March 2019

Published: 28 March 2019

C.D.M., M.F., S.R.S., and B.A. designed research; C.D.M. performed research; C.D.M., M.F., C.R.C., S.R.S., and B.A. contributed unpublished reagents/analytic tools; C.D.M. analyzed data; C.D.M., M.F., C.R.C., S.R.S., and B.A. wrote the paper.

Funding: Wellcome Trust (Wellcome)
Wellcome Trust NIH-fellowship
;

Funding: HHS | NIH | National Institute of Mental Health (NIMH)
ZIA MH002928-01
.

Conflict of Interest: Authors report no conflict of interest.

This work was supported by the Wellcome Trust NIH-fellowship (C.D.M., S.S., B.B.A.) and by NIH grant ZIA MH002928-01 (B.B.A.).

Correspondence should be addressed to Correspondance should be addressed to Christian D. Márton at cdmarton@gmail.com.

Cite as: eNeuro 2019; 10.1523/ENEURO.0467-18.2019

Alerts: Sign up at www.eneuro.org/alerts to receive customized email alerts when the fully formatted version of this article is published.

Accepted manuscripts are peer-reviewed but have not been through the copyediting, formatting, or proofreading process.

Copyright © 2019 Márton et al.
This is an open-access article distributed under the terms of the Creative Commons Attribution 4.0 International license, which permits unrestricted use, distribution and reproduction in any medium provided that the original work is properly attributed.

eNeuro Accepted Manuscript

eNeuro Accepted Manuscript

1) Manuscript Title

Signature patterns for top-down and bottom-up information processing via cross-frequency coupling in macaque auditory cortex

2) Abbreviated Title

Signature CFC patterns for bi-directional information processing in auditory cortex

3) Author Names

Christian D. Márton[1,2], Makoto Fukushima[2,3,4], Corrie R. Camalier[2], Simon R. Schultz[1], Bruno B. Averbeck[2]

1 Centre for Neurotechnology & Department of Bioengineering, Imperial College London, London, SW7 2AZ, United Kingdom; **2** Laboratory of Neuropsychology, Section on Learning & Decision Making, NIMH/NIH, Bethesda, MD, USA; **3** RIKEN Brain Science Institute, Saitama, Japan; **4** Consumer Neuroscience, The Nielsen Company, Tokyo, Japan

4) Author Contributions

CDM, MF, SRS, BBA Designed Research; CDM Performed Research; CDM, MF, SRS, BBA Contributed Analytic Tools; CDM Analyzed Data; CDM, MF, CRC, SRS, BBA Wrote Paper

5) Correspondance should be addressed to

cdmarton@gmail.com

6) Number of Figures: 16 (5 Main + 11 Supplementary)

7) Number of Tables: 0

8) Number of Multimedia: 0

9) Number of words for Abstract: 239

10) Number of words for Significance Statement: 103

11) Number of words for Introduction: 743

12) Number of words for Discussion: 1646

eNeuro Accepted Manuscript

13) Acknowledgements: None

14) Conflict of Interest: Authors report no conflict of interest

15) Funding Sources: This work was supported by the Wellcome Trust NIH-fellowship (C.D.M., S.S., B.B.A.) and by NIH grant ZIA MH002928-01 (B.B.A.).

eNeuro Accepted Manuscript

Signature patterns for top-down and bottom-up information processing via cross-frequency coupling in macaque auditory cortex

Abstract

Predictive coding is a theoretical framework that provides a functional interpretation of top-down and bottom up interactions in sensory processing. The theory suggests there are differences in message passing up vs. down the cortical hierarchy. These differences result from the linear feedforward of prediction errors, and the nonlinear feedback of predictions. This implies that cross-frequency interactions should predominate top-down. But it remains unknown whether these differences are expressed in cross-frequency interactions in the brain. Here we examined bi-directional cross-frequency coupling across four sectors of the auditory hierarchy in the macaque. We computed two measures of cross-frequency coupling, phase-amplitude coupling (PAC) and amplitude-amplitude coupling (AAC). Our findings revealed distinct patterns for bottom-up and top-down information processing among *cross*-frequency interactions. Both top-down and bottom-up made prominent use of low frequencies: low-to-low frequency (θ, α, β) and low frequency-to-*high* γ couplings were predominant *top-down*, while low frequency-to-*low* γ couplings were predominant *bottom-up*. These patterns were largely preserved across coupling types (PAC and AAC) and across stimulus types (natural and synthetic auditory stimuli), suggesting they are a general feature of information processing in auditory cortex. Our findings suggest the modulatory effect of low frequencies on γ-rhythms in distant regions is important for bi-directional information transfer. The finding of low frequency-to-*low* γ interactions in the bottom-up direction suggest non-linearities may also play a role in feedforward message passing. Altogether, the patterns of cross-frequency interaction we observed across the auditory hierarchy are largely consistent with the predictive coding framework.

1 Significance

The brain consists of highly interconnected cortical areas, yet the patterns in directional cortical communication are not fully understood, in particular with regards to interactions between different signal components across frequencies. We employed a novel, convenient and computationally advantageous Granger-causal framework to examine bi-directional cross-frequency interactions across four sectors of the auditory cortical hierarchy in macaques. Our findings reveal cross-frequency interactions are predominant in the top-down direction, with important implications for theories of information processing in the brain such as predictive coding. Our findings thereby extend the view of cross-frequency interactions in auditory cortex, suggesting they also play a prominent role in top-down processing.

eNeuro Accepted Manuscript

2 Introduction

One fundamental yet poorly understood component of cortical computation is the presence of widespread reciprocal cortical connections [Scott et al., 2015, Romanski and Averbeck, 2009, Kveraga et al., 2007, Salin and Bullier, 1995]. Moreover, most previous work has focused on the visual pathways. It remains unknown whether there are fundamental differences between top-down and bottom-up information processing along the auditory pathway. Cross-regional top-down effects in particular have remained unexplored, as most work has focused on bottom-up [Hyafil et al., 2015a, Giraud and Poeppel, 2012] or intra-regional effects [Lakatos et al., 2016]. In the present study, we examined bi-directional information processing across the macaque auditory hierarchy through an analysis of cross-frequency coupling (CFC). We computed two types of CFC measures, amplitude-amplitude (AAC) and phase-amplitude (PAC) coupling, for both natural and synthetic stimuli.

Cross-frequency coupling refers to correlation between the phase or amplitude component of one frequency and the amplitude component of other frequencies. This differs from linear analyses like coherence, which only examine coupling between signals at a single frequency. CFC, in contrast, considers interactions across the frequency spectrum. CFC may occur in several forms [Jirsa and Mueller, 2013] and has been observed during various tasks across several species including humans, macaques, and rodents. PAC, in particular, has received widespread attention. Coupling of low-frequency (e.g. θ, α) phase to high-frequency (e.g. γ) amplitude has been associated with various behavioral mechanisms including learning, memory and attention [Hyafil et al., 2015b, Colgin, 2015, Doesburg et al., 2012, Kendrick et al., 2011, Canolty and Knight, 2010, Tort et al., 2009, Tort et al., 2008, Cohen, 2008, Jensen and Colgin, 2007, Canolty et al., 2006, Schack et al., 2002]. The reason for interest in PAC is that it may offer a mechanistic account of information coordination across neural populations and timescales. The phase of low-frequency oscillations could modulate the amplitude of high-frequency oscillations, putatively allowing control of spiking activity [Buzsáki et al., 2012, Ray and Maunsell, 2011]. AAC has also been shown to correlate with behavior [Canolty and Knight, 2010], but has been less explored mechanistically. Here we obtained estimates of both PAC and AAC strength as measures of cross-regional information processing in the bottom-up and top-down direction, allowing the two measures to be contrasted and compared in terms of informational content.

One prevalent theory of information processing in the brain which separates bottom-up and top-down components is *predictive coding*. In this (Bayesian) view of the brain, expectations are formed about incoming sensory information. These top-down predictions (expectations) are compared with bottom-up sensory information (outcomes) and representations are then potentially updated based on a prediction error (surprise), which is the difference between sensory inputs and their expectations. Neural implementations of predictive

eNeuro Accepted Manuscript

coding suggest that predictions are formed in higher-order areas through a (linear) accumulation of prediction errors. The accumulation of prediction errors in higher-order areas results in the attenuation of high frequencies, thus feedforward connections can be cast as a low-pass or Bayesian filter. Conversely, prediction errors arising in lower-order areas are a non-linear function of predictions. This means high frequencies can be created in lower-order areas due to the inherent non-linearity. Hence, predictive coding implies that lower-order areas (where prediction errors arise) should display relatively higher frequencies (e.g. γ-range) than higher-order areas (where predictions are formed) [Bastos et al., 2012, Friston, 2008]. Several studies have supported this view [Michalareas et al., 2016, Bastos et al., 2015, Bastos et al., 2012, Fontolan et al., 2014], though not without exceptions.

It remains unknown whether this prediction is expressed in cross-frequency interactions in the brain. Here we probe this prediction by examining differences in cross-frequency coupling strength in the bottom-up and top-down direction across the frequency spectrum. Based on the predictive coding framework [Bastos et al., 2012, Friston, 2008], we would expect there to be an asymmetry between bottom-up and top-down interactions. This asymmetry arises due to the linear effect of prediction errors on predictions in the bottom-up direction, and the nonlinear effect of predictions on prediction errors in the top-down direction. Thus, we would expect nonlinear, *cross*-frequency interactions to predominate in the top-down direction.

Previous work has shown differences in how auditory cortical areas process natural and synthetic sounds [Fukushima et al., 2014]. It is possible that these differences translate into systematic differences in CFC patterns. If the revealed CFC pattern is a more general hallmark of inter-areal communication though, it should not be specific to stimulus type: natural and synthetic stimuli should show similar overall coupling patterns.

Our work revealed signature patterns of top-down and bottom-up processing in cross-regional PACs and AACs. These patterns were conserved across coupling types and across natural and synthetic stimuli. We found that low-to-low frequency (θ, α, β) and low frequency-to-*high* γ interactions were predominant *top-down*, while low frequency-to-*low* γ couplings were predominant *bottom-up*. Our findings suggest modulation of γ frequency power by low frequency rhythms plays a role in bi-directional information transfer across the auditory hierarchy. The finding of predominant cross-frequency interactions in the top-down direction across the auditory hierarchy largely agrees with the predictive coding framework.

eNeuro Accepted Manuscript

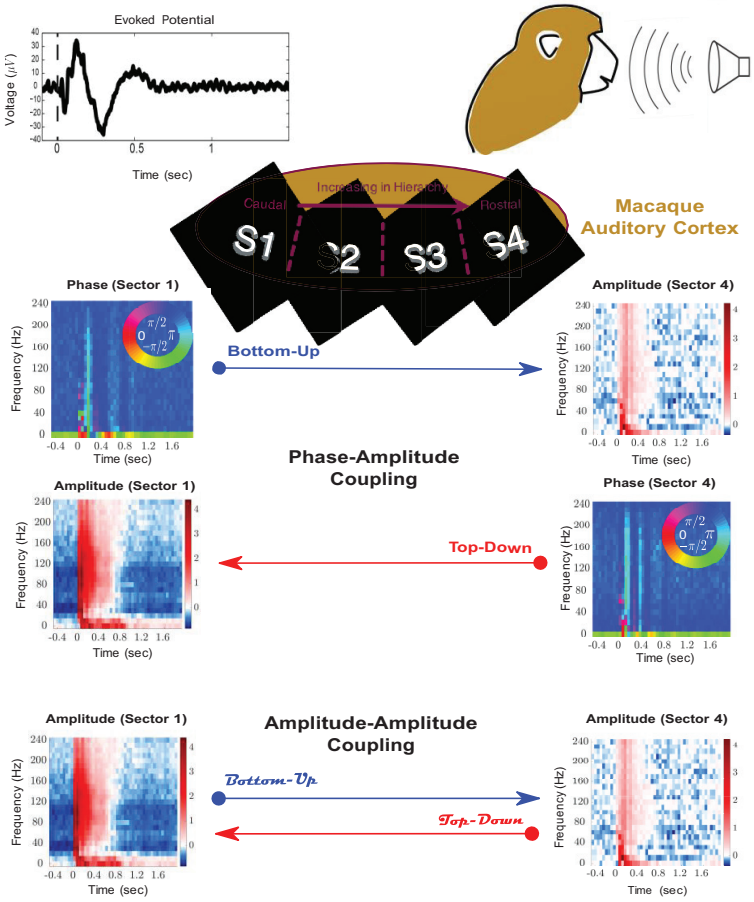

Fig 1. Coupling Analysis Overview: Recordings were made from four μECoG arrays spanning auditory cortex while monkeys listened to one of 20 natural vocalizations (VOC), 20 synthetic envelope-preserved sounds (EPSs) or 20 synthetic spectrum-preserved sounds (SPSs). Electrodes were partitioned into four sectors along the caudorostral axis (S1: A1/ML (primary auditory cortex/middle lateral belt), S2: R (rostral core region of the auditory cortex / AL (anterior lateral belt region of the auditory cortex), S3: RTL (lateral rostrotemporal belt region of the auditory cortex), S4: RTp (rostrotemporal pole area)). We decomposed the signal into its time-frequency representation, and obtained amplitude and phase components for each sector. We investigated two types of coupling across sectors: amplitude-amplitude and phase-amplitude coupling. We computed both types of coupling in the bottom-up and top-down direction. Top-down coupling was defined as coupling in which the source electrode came from a sector of higher order than the target electrode, and vice versa for bottom-up coupling.

eNeuro Accepted Manuscript

3 Methods and Materials

3.1 Subjects

Three adult male rhesus monkeys (Macaca mulatta) weighing 5.5–10 kg were used for recordings. All procedures and animal care were conducted in accordance with the Institute of Laboratory Animal Resources Guide for the Care and Use of Laboratory Animals. All experimental procedures were approved by the National Institute of Mental Health Animal Care and Use Committee.

3.2 Stimuli

The stimuli used for the main experiment included 20 conspecific monkey vocalizations (VOC) and two sets of 20 synthetic stimuli each (envelope-preserved sound, EPS; and spectrum preserved sound, SPS) derived from the original VOC stimuli. The VOC stimulus set consisted of 20 macaque vocalizations employed in previous studies [Kikuchi et al., 2010, Fukushima et al., 2014].

In order to obtain EPS from VOC stimuli, the envelope of a particular vocalization was estimated based on the amplitude component of the original stimulus' Hilbert transform. The amplitude envelope was then multiplied by broadband white noise to create the EPS stimulus. Thus, all 20 EPS stimuli exhibited flat spectral content; these stimuli could not be discriminated based on spectral features, while the temporal envelopes (and thus the durations) of the original vocalizations were preserved.

SPS stimuli were obtained by first generating broadband white noise with a duration of 500 ms and computing its Fourier transform. The SPS stimulus' amplitude in the Fourier domain was then replaced by the average amplitude of the corresponding VOC stimulus, before transforming back to the time domain by computing the inverse-Fourier transform. This resulted in a sound waveform that preserved the average spectrum of the original vocalization, while exhibiting a flat temporal envelope, random phase, with a duration of 500 ms. A 2 ms cosine rise/fall was then imposed on the stimulus to avoid abrupt onset/offset-effects. Hence, all 20 SPS stimuli exhibited nearly identical, flat temporal envelopes; these stimuli could not be discriminated using temporal features, while the average spectral power of the original vocalizations was preserved.

A total of 60 different stimuli were presented in pseudorandom order, with an interstimulus interval of 3 s. Each stimulus was presented 60 times. The sound pressure levels of the stimuli measured by a sound level meter ranged from 65 to 72 dB at a location close to the animal's ear. Stimulus duration ranged from around .15 to 1 second [Fukushima et al., 2014].

eNeuro Accepted Manuscript

3.3 Recordings

Custom-designed μECoG arrays (NeuroNexus Technologies, MI, USA) were used to record field potentials from macaque auditory cortex. Arrays were machine fabricated on a very thin polyimide film (20 μm), with each array featuring 32 recording sites, 50 μm in diameter each, on a 4 x 8 grid with 1 mm spacing (i.e., 3 x 7 mm rectangular grid). Two animals, monkeys B and K, were implanted with arrays each in the left hemisphere, while one animal, monkey M, was implanted with arrays in the right hemisphere. Three of the arrays in each monkey were placed on top of STP, in a caudorostrally oriented row.

To implant the arrays, we removed a frontotemporal bone flap extending from the orbit ventrally toward the temporal pole and caudally behind the auditory meatus and then opened the dura to expose the lateral sulcus. The most caudal of the three ECoG arrays on the STP was placed first and aimed at area A1 by positioning it just caudal to an (imaginary) extension of the central sulcus and in close proximity to a small bump on the STP, both being markers of A1's approximate location. Each successively more rostral array was then placed immediately adjacent to the previous array to minimize interarray gaps. The arrays on the lateral surface of the STG were placed last. The probe connector attached to each array was temporarily attached with cyanoacrylate glue or Vetbond to the skull immediately above the cranial opening. Ceramic screws together with bone cement were used to fix the connectors to the skull. The skin was closed in anatomical layers. Post- surgical analgesics were provided as necessary, in consultation with the National Institute of Mental Health veterinarian.

3.4 Stimulus presentation and recording parameters

The monkey was placed in a sound-attenuating booth for the experiment (Biocoustics Instruments). The sound stimuli were presented while the monkey sat in a primate chair and listened passively with its head fixed. Auditory evoked potentials from the 128 channels of the ECoG-array were bandpassed between 2-500 Hz, digitally sampled at 1500 Hz, and stored on hard-disk drives by a PZ2–128 preamplifier and the RZ2 base station (Tucker Davis Technology).

3.5 Data Pre-Processing

Data analysis was performed using MATLAB R2017a (MathWorks) software. Since there was little significant auditory evoked power above 250 Hz, recordings were low-pass filtered and resampled at 500 Hz to enhance calculation speed and reduce memory requirements. The signal was bandpassed at 60Hz with a narrow-band filter to eliminate the possible presence of line-noise; a 6th-order Butterworth filter was chosen to achieve a sharp dropoff in the stop-band, thus minimizing the effect of the filter on neighboring frequency bands.

eNeuro Accepted Manuscript

The 96 sites on the supratemporal plane (STP) were grouped based on the characteristic frequency maps obtained from the high-gamma power of the evoked response to a set of pure-tone stimuli. The change in frequency tuning along the STP reverses across areal boundaries, and these reversals were therefore used to identify the areal boundaries. This resulted in a grouping of electrodes into four sectors (Fig 1), which were estimated to correspond to the following subdivisions at a caudorostral-level within macaque auditory cortex: Sec (Sector) 1, A1/ML (primary auditory cortex/ middle lateral belt); Sec 2, R (rostral core region of the auditory cortex)/AL (anterior lateral belt region of the auditory cortex); Sec 3, RTL (lateral rostrotemporal belt region of the auditory cortex); Sec 4, RTp (rostro-temporal pole area). The recorded signal from each site partitioned into sectors 1-4 was re-referenced by subtracting the average of all sites within a particular sector [Fontolan et al., 2014, Kellis et al., 2010].

We defined the following terminology to refer to particular frequency spaces throughout this paper: *delta* (δ) range: 0 - 2.5 Hz; *theta* (θ) range: 2.5 - 7.5 Hz; *alpha* (α) range: 7.5 - 12.5 Hz; *low beta* (*low* β) range: 12.5 - 22.5 Hz; *high beta* (*high* β) range: 22.5 - 42.5 Hz; *low gamma* (*low* γ) range: 42.5 - 67.5 Hz; *high gamma* (*high* γ) range: > 67.5 Hz. The delta frequency band (0 - 2.5 Hz) was not included in the analysis since the pre-amplifier employed during the recording sessions does not allow for recording frequency components below 2 Hz and the power in this band was expectedly low.

3.6 Phase-amplitude (PAC) and amplitude-amplitude (AAC) cross-frequency coupling (CFC) Calculation

3.6.1 Frequency Transformation

For Figures 1-5, the field potential data was first transformed into frequency space by computing the fast Fourier transform (FFT) of the signal in every channel using a 200 ms Hanning window, stepped by 200 ms. Thus, we obtained a frequency representation of the data at a 5Hz bandwidth ranging from 2.5Hz - 132.5Hz, which satisfies the Nyquist-criterium. We obtained the phase and amplitude information in a given source and target region for every channel and normalized the amplitude information in each frequency band by the corresponding power in that frequency band, averaged across the entire experiment, so as to account for decreasing power with frequency (Fig. 2-1).

3.6.2 Obtaining CFCs using canonical correlation

We computed two types of cross-frequency coupling, phase-amplitude (PAC) and amplitude-amplitude (AAC) coupling. Couplings were calculated for every channel pair across the four sectors (S1-S4), resulting in 6 possible

eNeuro Accepted Manuscript

cross-sector pairs (S1-S2, S1-S3, S1-S4, S2-S3, S2-S4, S3-S4). We obtained estimates of coupling strength in two directions, bottom-up and top-down. In the former case, the source component was derived from a recording site in a sector lower in the auditory hierarchy than the target component (referred to as bottom-up coupling), while in the latter case the source component came from a sector higher in the auditory hierarchy than the target component (referred to as top-down coupling) (Fig. 1). Ultimately, we were interested in examining the difference in coupling strength in the top-down and bottom-up directions across the auditory hierarchy. Results are presented collapsed across all cross-sector pairs (Fig. 2), as well as separately for every cross-sector pair (Fig. 3), averaged across all channel pairs and across the three animals in both cases.

We used canonical correlation analysis (CCA), to compute both types of coupling. The advantage of CCA is that it computes coupling among multivariate observations in the source and target regions. This framework, therefore, allows CFC values to be computed across the entire frequency range simultaneously. Furthermore, some approaches to calculating AAC and PAC first carry out dimensionality reduction on the source and target region signals separately, and then calculate correlations in the low dimensional space. If the variance preserving dimensions in the source and target space are not the dimensions that maximize correlations between the source and target space, interactions may be missed. CCA on the other hand finds the low dimensional representations that maximize coupling between the source (X) and target (Y) space. In CCA, one is seeking projections (linear combinations) $U = XA$ and $V = YB$ such that the correlation $corr(U, V)$ among these derived directions is maximal [Durstewitz, 2017].

We carried out our analyses using a Granger Causal framework. Therefore, we first carried out CCA between amplitude in the target region and time lagged versions of the amplitude also within the target region, obtaining an estimate of the the coupling strength $\hat{Y}$ that could be inferred purely from coupling of the signal at the target electrode onto itself. For computational reasons, we used two time lags to estimate the target signal (we found that using one time lag did not affect our results). More explicitly, we transformed the current and lagged signal into the frequency domain as described above and computed the canonical correlation between the lagged components and the current signal in the target. We used the first canonical value only to obtain $\hat{Y}$ (results did not differ from those obtained from including more entries). We then obtained the residual $\tilde{Y}$ from this analysis, and used this residual when we examined the interactions between regions. Subsequent analysis was performed using the residuals $\tilde{Y}$ from this regression as the signal for the target region.

We then computed phase-amplitude (PAC) and amplitude-amplitude (AAC) cross-frequency couplings across the four sectors (Fig. 1), by regressing the phase or amplitude component of the signal from the source sector, respectively, on the amplitude component of the signal in the target sector for every channel. More specifically, we calculated instantaneous coupling in 200ms windows between source and target region for each

eNeuro Accepted Manuscript

electrode pair. PAC and AAC was calculated in the CCA framework across all time windows and trials altogether, simultaneously across all frequency bands. In the case of PAC, $X_{n \times d1}$ contained the sine and cosine transformed phase component of the signal, while $Y_{n \times d2}$ contained the squared and log-transformed amplitude component of the signal, with $n = 10800$ (1200 trials * 9 windows) observations for VOC and SPS stimuli and $n = 10773$ observations (1197 trials * 9 windows) for EPS stimuli, $d2 = 25$, and $d1 = 25$ or $d1 = 25 * 2$ for PAC and AAC, respectively (Eq 1).

After obtaining the canonical coefficient matrices $B_{d2 \times d}$ and $A_{d1 \times d}$ within the CCA framework (Eq 1), one can obtain the coupling matrix $P_{d2 \times d1}$ by multiplying the B and A matrices with the canonical values S of the correlation matrix (Eq 2). We used the first 10 directions ($d = 10$) that captured most of the interaction; results did not differ from those obtained from including all entries. For AAC, the final cross-frequency coupling matrix is P. For PAC, one combines the sine and cosine components of P by computing their Euclidian norm, yielding the final coupling matrix $P^*_{d2 \times d1}$ with $d2 = d1$.

$$U_{n \times d} = X_{n \times d1} A_{d1 \times d}, \quad V_{n \times d} = Y_{n \times d2} B_{d2 \times d}, \quad \underset{A,B}{\operatorname{argmax}} \{corr(U, V)\} \tag{1}$$

$$P_{d2 \times d1} = BSA^T, \quad P^*_{d2 \times d1} = \begin{bmatrix} \sqrt{P_1^2 + P_{m/2}^2} \\ \dots \\ \sqrt{P_{m/2}^2 + P_m^2} \end{bmatrix} \tag{2}$$

3.6.3 Obtaining the difference between top-down (TD) and bottom-up (BU) coupling

We obtained AAC and PAC coupling matrices in this manner for both the bottom-up and the top-down direction. In bottom-up coupling, the source component was derived from a recording site in a sector lower in hierarchy than the target component (referred to as bottom-up coupling), while in top-down coupling, the source component came from a sector higher in hierarchy than the target component (Fig. 1). We then obtained the difference $\Delta P_{same\ stim}$ between the top-down and bottom-up coupling matrices $P_{Top-Down}$ and $P_{Bottom-Up}$ (Eq 3). This was done separately for each of the cross-sector pairs. Results are presented collapsed across all cross-sector pairs (Fig. 2), as well as separately for every cross-sector pair (Fig. 3).

$$\Delta P = P_{Top-Down} - P_{Bottom-Up} \tag{3}$$

eNeuro Accepted Manuscript

3.6.4 Obtaining the difference in coupling strength between original (VOC) and synthetic stimuli (EPS/SPS)

In order to examine the difference in coupling strength between natural and synthetic stimulus types (Fig. 4,5), we computed the difference between VOC and EPS stimuli (Fig. 4) and between VOC and SPS stimuli (Fig. 5) separately in the top-down (TD, Eq 4) and bottom-up direction (BU, Eq 5).

$$\Delta P^{TD}_{VOC\ vs\ Synthetic} = P^{TD}_{VOC} - P^{TD}_{EPS/SPS} \quad (4)$$

$$\Delta P^{BU}_{VOC\ vs\ Synthetic} = P^{BU}_{VOC} - P^{BU}_{EPS/SPS} \quad (5)$$

3.7 Statistical Analysis

Paired t-tests were performed to establish statistical significance of the difference between top-down and bottom-up coupling (ΔP; Fig. 2, Fig. 3, Fig. 4), as well as the differences between original and synthetic stimuli ($\Delta P^{TD}_{VOC\ vs\ Synthetic}$, $\Delta P^{BU}_{VOC\ vs\ Synthetic}$; Fig. 5). This was done separately for each frequency pair, by testing whether the mean of the difference between top-down and bottom-up coupling (or the difference between original and synthetic stimuli in each direction) was significantly different from zero (null hypothesis). Lilliefors' test for normality was conducted for each frequency pair in order to ensure the normality assumption was satisfied, and histogram plots were inspected for select frequency pairs (Fig. 2-2, 2-3).

More specifically, in order to assess overall differences in coupling strength between the two directions (Fig. 2, Fig. 4) and to assess differences in coupling strength between natural and synthetic stimuli (Fig. 5), paired t-tests were conducted across all channel pairs, cross-regional pairs and animals altogether (*d.f.* = 9344). In order to assess coupling differences for each regional pair separately (Fig. 3), paired t-tests were conducted separately for each regional pair, across all channel pairs and animals altogether (*d.f.* = 1056).

Significant phase-amplitude and amplitude-amplitude coupling (highlighted by black outlines throughout the manuscript) was based on corrected p-values using non-parametric permutation tests that generated null distributions of the maximum cluster size [Maris and Oostenveld, 2007, Nichols and Holmes, 2001]. This procedure implicitly adjusts for searching over multiple frequencies. The null distribution was obtained by randomly reassigning electrodes to source or target region and recalculating differences in coupling strength for 100 repeats. Clusters of the 99th percentile (corresponding to $p \leq 0.01$) were considered significant and are reported throughout the manuscript (marked by black outlines).

eNeuro Accepted Manuscript

4 Results

We analyzed local field potentials recorded simultaneously from multiple cortical areas in the auditory cortex of three macaques while the animals listened to auditory stimuli (Fig. 1). These auditory stimuli consisted of 20 natural conspecific vocalizations, 20 envelope-preserved stimuli (EPS) and 20 spectrum-preserved stimuli (SPS), which were derived from the original vocalizations [Fukushima et al., 2014]. A previous study established the approximate rostrocaudal location of implanted micro-electrocorticography (μECoG) arrays along the auditory hierarchy by the characteristic frequency of each electrode contact [Fukushima et al., 2012, Fukushima et al., 2014]. This partitioned the recording sites into four sectors (S1-S4), putatively spanning the caudorostral levels from the core A1 (S1) to RTp (S4), including some of the surrounding belt areas (Fig. 1). We operationally defined feedforward to occur from earlier to later sectors (bottom-up direction), and feedback to occur from later to earlier sectors (top-down direction).

We wanted to examine cross frequency interactions across the auditory hierarchy. To characterise phase-amplitude and amplitude-amplitude coupling, we first decomposed the signal into its spectral component using the short-time fast Fourier transform and obtained phase and amplitude components (Fig. 1). We then used canonical correlation analysis (CCA) to parameterise the cross-frequency coupling under a general linear model (Methods and Materials). The fluctuations in amplitude in the target sector were predicted based on instantaneous amplitude fluctuations in the source sector within 200ms windows. Furthermore, the target and source time series were adjusted to remove the effect of predicted fluctuations from the target region. In other words, by appealing to the notion of Granger causality, a significant mapping between the source and the target - that cannot be explained by the history of the target - is evidence of (cross-frequency) coupling.

We computed coupling strength across the frequency spectrum for each cross-regional pair, separately in the top-down and bottom-up direction (Fig. 1). Top-down coupling was defined as coupling in which the source electrode came from a sector of higher order than the target electrode, and vice versa for bottom-up coupling. For example, coupling between the phase (or amplitude) in S4 and the amplitude in S1 is defined as top-down, and coupling between the phase (or amplitude) in S1 and the amplitude in S4 is defined as bottom-up in the case of PAC (or AAC). This definition is in accordance with a previous approach [Fontolan et al., 2014].

4.1 Distinct cross-frequency coupling signatures for bottom-up and top-down coupling, both involving low frequencies

We first examined PAC and AAC across the four sectors, in auditory evoked potentials to 20 conspecific vocalizations (VOC). Both CFC measures peaked in the θ frequency range and showed relatively strong coupling

eNeuro Accepted Manuscript

across all the target amplitude frequencies (Fig. 2A,B,D,E). The field potential signal showed the highest power in the same frequency band decaying with the typical $1/f$ pattern thereafter (Fig 2-1), thus satisfying a pre-requisite for the presence of physiologically meaningful CFC [Aru et al., 2015].

Among PACs, both top-down and bottom-up coupling was dominant between θ phase and broadband amplitude (Fig. 2A,B). Examining differences in coupling strength in the two directions more closely (Fig. 2C), PACs showed dominant top-down coupling in the low-frequency space (θ, α, β phase to θ, α, β amplitude), as well as between low frequency phase and high-γ (>67.5Hz) amplitude ($p \leq 0.01$, cluster-corrected). Bottom-up PAC was dominant between low frequency phase (θ, α, β) and low-γ (47.5-62.5Hz) amplitude ($p \leq 0.01$, cluster-corrected).

AACs showed a similar pattern to PACs in both directions, but coupling strength and differences in coupling strength were overall by an order of magnitude lower than for PACs (Fig. 2D,E). AACs replicated the pattern observed in PACs, with dominant θ to broadband coupling in both directions. Additionally, and unlike in PACs, coupling strength among same-frequency couplings was pronounced in both directions with strongest coupling in the low-frequency range (Fig. 2D,E). Examining differences in coupling strength in the two directions more closely (Fig. 2F), AACs displayed a similar pattern to PACs but showed smaller significant clusters than PACs across the entire frequency spectrum.

eNeuro Accepted Manuscript

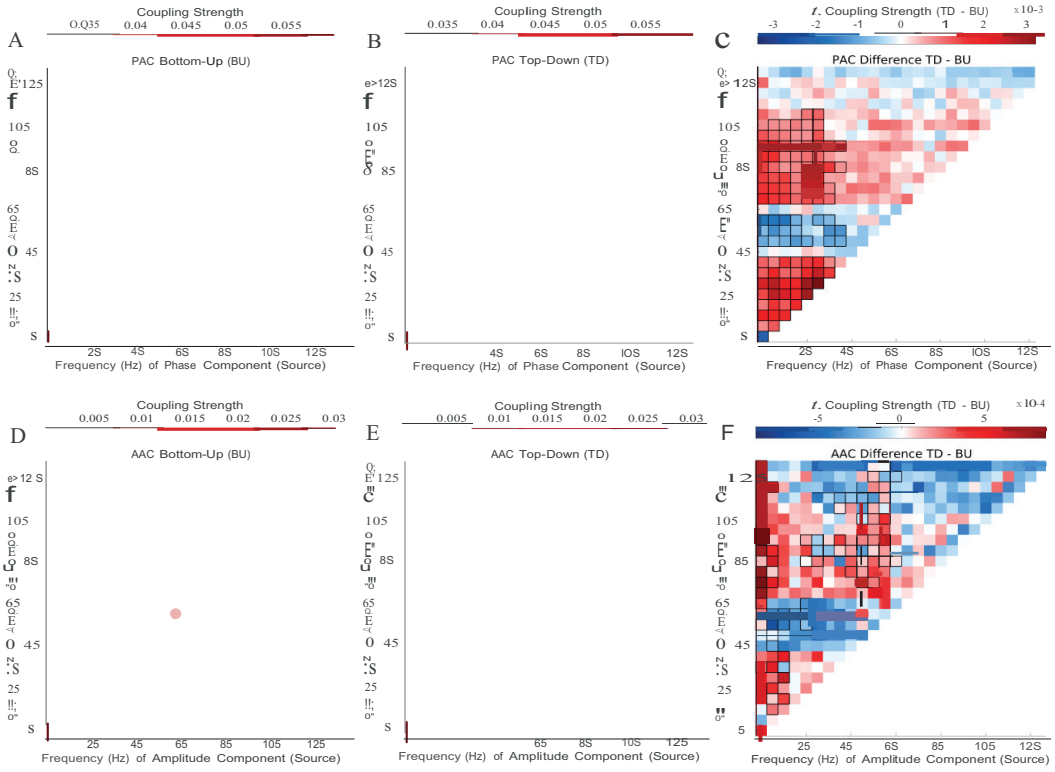

Fig 2. Top-down vs. bottom-up phase-amplitude and amplitude-amplitude coupling in natural vocalizations (VOC). (A-B) Phase-amplitude coupling (PAC) strength in the top-down (A) and bottom-up direction (B). Depicted are canonical correlation-derived coupling coefficients (see Methods and Materials). (C) Difference in top-down and bottom-up in PAC strength. Significant differences are enclosed by black rectangles (p:::;0.01, cluster-corrected). (D-E) Amplitude-amplitude coupling (AAC) strength in the top-down (D) and bottom-up direction (E). Depicted are canonical correlation-derived coupling coefficients. (F) Difference between top-down and bottom-up in AAC strength. Significant differences are enclosed by black rectangles (p:::;0.01, cluster-corrected). Results are depicted averaged across all channels, cross-regional pairs, and animals. Supporting Figures: Fig. 2-1, 2-2, 2-3

4.2 Cross-regional coupling mainly driven by interactions between Al and higher order sectors

To examine cross-regional patterns in coupling across the auditory hierarchy (Fig. 1) more closely, we analyzed differences between top-down and bottom-up coupling strength separately across the six cross-regional pairs (Fig. 3). This revealed that the overall coupling pattern (Fig. 2) was mostly driven by interactions between S1 (A1/ML) and S2-S4 (higher-order sectors) (Fig. 3 A,B,C), rather than by interactions among higher-order sectors

eNeuro Accepted Manuscript

(Fig. 3 D,E,F).

More specifically, interactions between S1 (A1/ML) and S2 (R/AL)/ S3 (RTL) / S4 (RTp) show dominant top-down coupling of low frequency phase to low and high frequency amplitude (Fig. 3A-C), whereas these asymmetries are largely absent among interactions between S2-S4 (Fig. 3D-F). The interaction between S1 and S2 (Fig. 3B) shows overall less widespread top-down coupling strength compared to interactions between S1 and S3/S4. The full pattern (as manifested in Fig. 2) only gains full prominence among cross-regional pairs S1-S4 (Fig. 3C), which also includes predominant bottom-up coupling between low frequency phase and low-γ amplitude. Interactions between higher-order sectors (Fig. 3 D,E,F) show fewer differences between top-down and bottom-up coupling, but they do show predominant bottom-up coupling between low frequency phase and low-γ amplitude (Fig. 3 E,F). A similar trend was observed among AACs, though differences were overall smaller and less widespread compared to PACs (Fig. 3-1).

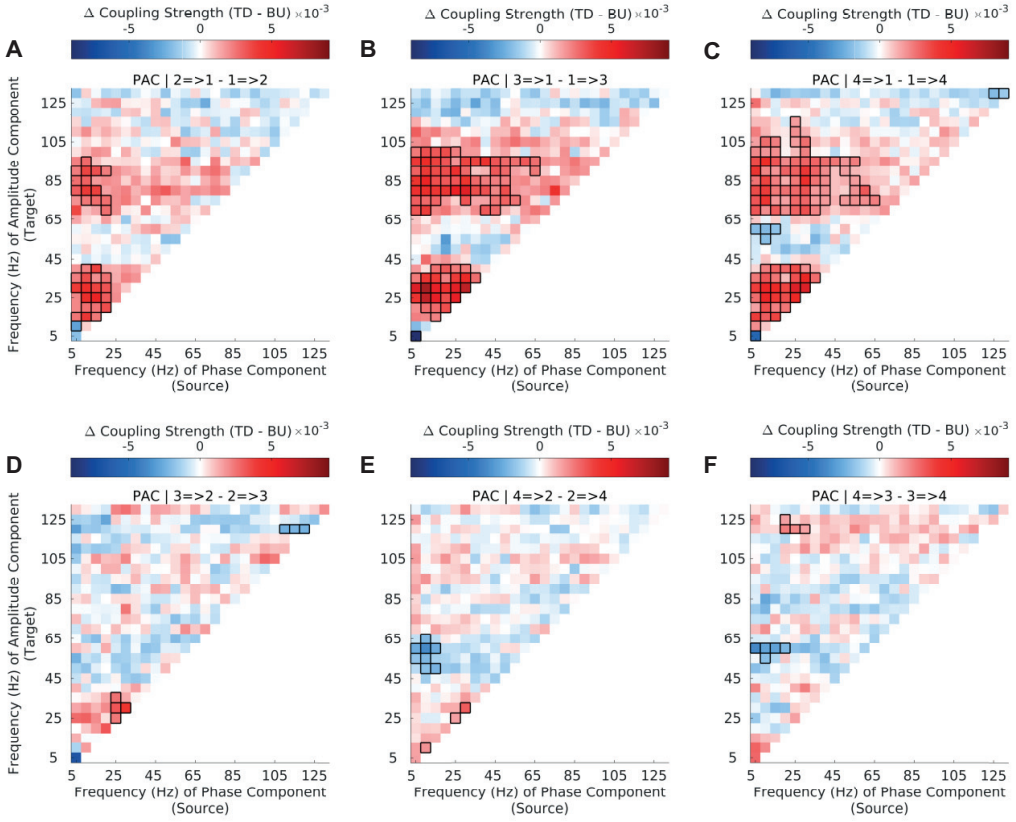

eNeuro Accepted Manuscript

Fig 3. Top-down versus bottom-up phase-amplitude coupling strength (PAC) across the auditory hierarchy in natural stimuli Difference in top-down and bottom-up *phase-amplitude* coupling (PAC) strength for CFC between sectors 1 (A1/ML) and 2 (R/AL) **(A)**, sectors 1 (A1/ML) and 3 (RTL) **(B)**, sectors 1 (A1/ML) and 4 (RTp) **(C)**, sectors 2 and 3 **(D)**, sectors 2 and 4 **(E)** and sectors 3 and 4 **(F)** (see Methods and Materials 3.5 for sector definitions). Interactions between sector 1 (A1/ML) and higher order sectors show strong asymmetries in bottom-up and top-down coupling strength across the frequency spectrum; interactions among higher-order sectors (S2-S4) show less widespread asymmetries. Significant differences are enclosed by black rectangles ($p \leq 0.01$, cluster-corrected). Results are depicted averaged across all channels and animals. Supporting Figures: Fig. 3-1.

4.3 Top-down and bottom-up cross-frequency signatures generalize to synthetic stimuli

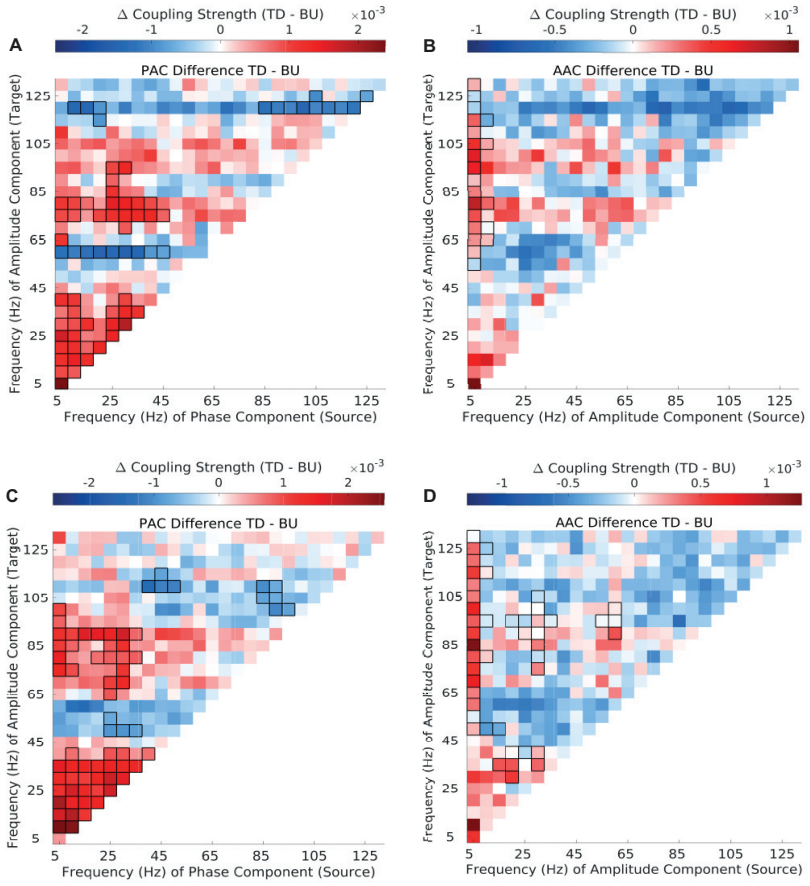

eNeuro Accepted Manuscript

Fig 4. Top-down vs. bottom-up phase-amplitude and amplitude-amplitude coupling in synthetic envelope-preserved stimuli (EPS) and synthetic spectrum-preserved stimuli (SPS) (A) Difference in top-down and bottom-up PAC strength in EPS stimuli. **(B)** Difference in top-down and bottom-up AAC strength in EPS stimuli. **(C)** Difference in top-down and bottom-up PAC strength in SPS stimuli. **(D)** Difference in top-down and bottom-up AAC strength in SPS stimuli. Significant differences are enclosed by black rectangles ($p \leq 0.01$, cluster-corrected). Results are depicted averaged across all channels, cross-regional pairs, and animals. Supporting Figures: Fig. 4-1, 4-2, 4-3, 4-4, 4-5, 4-6

To examine whether the observed coupling patterns are a general feature of inter-areal communication, we also analyzed coupling strength in two types of synthetic stimuli derived from the natural vocalizations. Envelope-preserved sounds (EPS) were obtained by leaving the original temporal envelope of the vocalization intact but flattening its spectral content, while spectrum-preserved sounds (SPS) were obtained by leaving the spectral information of the original vocalization intact but flattening its temporal envelope [Fukushima et al., 2014] (see Methods and Materials 3.2).

EPS and SPS stimuli showed similar bottom-up and top-down coupling patterns to natural stimuli, with pronounced θ-to-broadband coupling strength in both directions (Fig. 4-1,4-4). Examining differences between top-down and bottom-up coupling strength in both types of synthetic stimuli (Fig. 4,4-1, 4-4), we found that they reflected the same coupling asymmetries across the frequency spectrum as natural stimuli did (Fig. 2). This was true for PAC (Fig. 4A,C) and AAC (Fig. 4B,D) alike. More specifically, both types of synthetic stimuli showed dominant top-down coupling among low-to-low frequency and low-to-high γ interactions, and dominant bottom-up coupling among low-to-low γ interactions, like natural stimuli did. Both types of synthetic stimuli also showed similar coupling asymmetries to natural stimuli when examining cross-regional pairs separately (Fig. 4-2, 4-3, 4-5, 4-6), with most of the pattern driven by interactions between A1 and higher-order sectors rather than interactions among higher-order sectors, as in natural vocalizations.

4.4 Synthetic stimuli show overall lower bi-directional coupling than natural stimuli

To examine differences in coupling strength between natural and synthetic stimuli more closely, we compared coupling strength across stimuli separately in the top-down and bottom-up direction (Fig. 5).

EPS stimuli showed overall lower coupling strength than natural stimuli in both directions for both PACs and AACs (Fig. 5). Among PACs more specifically (Fig. 5A-B), natural stimuli showed higher coupling strength in the top-down direction for select frequency pairs in the low frequency space as well as among low frequency to high-γ couplings (Fig. 5A). In the bottom-up direction, coupling strength for natural stimuli was enhanced among low frequency to low and high γ couplings (Fig. 5B). In the bottom up direction, there were also select coupling values in the high γ frequency target amplitude space for which coupling was stronger in EPS stimuli.

eNeuro Accepted Manuscript

Among AACs, coupling strength was increased for natural compared to EPS stimuli across the entire frequency spectrum in both directions (Fig. 5 E-F). In particular, *B-1* amplitude-amplitude interactions were significantly lower for EPS stimuli in both directions. Altogether, coupling strength is enhanced for natural stimuli over envelope-preserved but spectrally flat synthetic stimuli (EPS) in both directions and across the entire frequency spectrum.

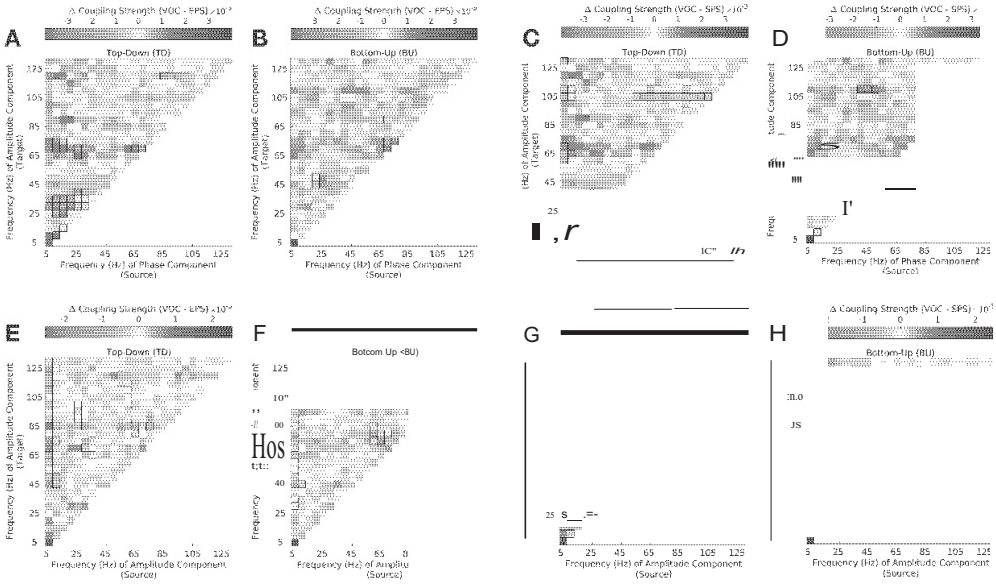

Fig 5. Phase-amplitude and amplitude-amplitude coupling strength in natural vocalizations (VOC) compared to synthetic envelope-preserved sounds (EPS) and spectrum-preserved sounds (SPS) (A-B) Difference in PAC strength between natural (VOC) and synthetic envelope-preserved sounds (EPS), separately in the top-down (B) and bottom-up direction (C). (C-D) Difference in AAC strength between VOC and EPS, separately in the top-down (C) and bottom-up direction (D). Significant differences are enclosed by black rectangles (p:S;O.Ol, cluster-corrected). Results are depicted averaged across all channels, cross-regional pairs, and animals. Supporting Figures: Fig. 5-1

SPS stimuli also showed overall lower coupling strength compared to natural stimuli. Among PACs, SPS stimuli showed lower coupling strength for select low-to-low and low-to- high frequency couplings in both directions (Fig. 5C,D). In the top-down direction, SPS stimuli showed higher coupling strength among 1-1 interactions (Fig. 5D). SPS and natural stimuli displayed similar differences among AACs (Fig. 5G,H). Altogether, coupling strength was mostly increased for natural compared to to SPS stimuli across the entire frequency spectrum in both directions.

Comparing SPS and EPS stimuli directly (Fig. 5-1), coupling strength was largely reduced for EPS stimuli across the frequency spectrum in both directions among PACs (Fig. 5-lA,B). This was also true among AACs

eNeuro Accepted Manuscript

(Fig. 5-1C,D), though there were fewer differences here than among PACs, especially in the high frequency space.

Overall, top-down and bottom-up cross-frequency coupling signatures were preserved among synthetic stimuli, albeit at overall reduced coupling strength.

5 Discussion

We found distinct cross-frequency signatures for top-down and bottom-up information processing in auditory cortex. These patterns were similar across phase-amplitude and amplitude-amplitude couplings, and across stimulus types (albeit at lower coupling strength in synthetic spectrum-flat stimuli). More specifically, we observed dominant top-down coupling among low-to-low and low-to-high γ frequency interactions, and dominant bottom-up coupling among low-to-low γ frequency interactions. These patterns were largely preserved across coupling types (PAC and AAC) and across stimulus types (natural and synthetic stimuli), and mostly driven by interactions between A1 and higher-order sectors. Differences in coupling strength across the auditory hierarchy are overall by an order of magnitude smaller among AACs than among PACs. Although the observed effects are subtle, they are significant and highly preserved. Altogether, our results suggest these cross-frequency signatures are a general hallmark of bottom-up and top-down information processing in auditory cortex.

The top-down coupling profile we observed is in accordance with previous results, but we also observed predominant low frequency to *low* γ coupling in the bottom-up direction. Previous studies found that feedforward (or bottom-up) influences were mediated by gamma frequency range rhythms [Michalareas et al., 2016, Bastos et al., 2015, Fontolan et al., 2014, Bosman et al., 2012]. However, across each of these studies, there were examples of a broader frequency range being employed for bottom-up information transmission. [Fontolan et al., 2014] reported higher bottom-up coupling of delta (1-3Hz) frequency phase in left A1 to high gamma (80-100Hz) amplitude in left association auditory cortex using human depth recordings. [Bastos et al., 2015] found that theta-channels were being used in addition to gamma-frequency channels in feedforward information transmission among primate visual areas. Finally, [Michalareas et al., 2016] did not observe stronger alpha-beta frequency range feedback (top-down) modulation in 8 out of 21 primate visual cortex area pairs (with 2 pairs showing the opposite pattern), and no stronger gamma frequency range feedforward (bottom-up) modulation in 5 out of 21 pairs. We observed predominant bottom-up coupling between low frequency (θ,α,β) phase (or amplitude) and low-γ amplitude among phase-amplitude couplings (and amplitude-amplitude couplings,respectively). Differences in exact frequency ranges reported may be due to regional (visual versus auditory cortex) variation [Tort et al., 2009, Canolty et al., 2006] and species-related variation. Overall, our findings agree with accounts of predominant low-to-high (cross-)frequency interactions top-down. But together with the exceptions above, our findings suggest

eNeuro Accepted Manuscript

low-to-high (cross-)frequency interactions may also play a role in bottom-up processing, pointing to a picture of top-down and bottom-up processing that is more complex than the previously hypothesized 'β-down vs. γ-up'.

Bottom-up PAC can be relevant to stimulus encoding. For example, an oscillation-based theory of speech encoding [Hyafil et al., 2015a, Giraud and Poeppel, 2012] predicts that cortical theta oscillations track the syllabic rhythm of speech and, in turn, reset the spiking of neurons at a gamma frequency level through θ-γ PAC. This ensures that neural excitability is optimally aligned with incoming speech. Our finding of dominant low frequency phase to γ amplitude coupling bottom-up fits within a framework that requires theta-gamma coupling for accurate speech encoding [Hyafil et al., 2015a]. Cross-regional θ-γ PAC as we observed here across A1 and higher order sectors could be responsible for coordinating information processing along the auditory cortical hierarchy. Our observation that these patterns are consistent across stimulus classes implies that this may be a generalized mechanism of auditory information processing which is co-opted during speech processing. However, our finding of enhanced low-to-high frequency phase-amplitude coupling in the top-down direction shows these couplings also mediate top-down influences on information processing.

Coupling in the top-down direction has been of particular interest in theories of the effect of attention on auditory information processing. Attention is thought to sample stimuli rhythmically, fluctuating at a 4-10 Hz rhythm [Landau and Fries, 2012], and was shown to enhance the processing of degraded speech in the anterior and posterior STS [Wild et al., 2012]. Frontal top-down signals in the delta and theta frequency range have been shown to modulate low-frequency oscillations in human auditory cortex, increasing their coupling to continuous speech [Park et al., 2015]. The same delta and theta frequency bands have been shown to be more strongly coupled to gamma-range burst rate within monkey A1 during periods of task entrainment [Lakatos et al., 2016]. In visual cortex, delta frequency oscillations have been shown to entrain with the rhythm of stimuli in the attended stream [Schroeder et al., 2010, Lakatos et al., 2008], and top-down beta-band modulation was found to be enhanced with attention [Bastos et al., 2015]. Increased power in low-frequency range oscillations may also, in turn, enhance bottom-up rhythms through top-down (cross-frequency) coupling [Bressler and Richter, 2015, Lee et al., 2013]; indeed, top-down beta-band activity was found to be maximally correlated with bottom-up gamma-band activity when top-down preceded bottom-up activity [Richter et al., 2017]. In addition, top-down couplings may also reflect the modulatory activity of predictive processes on auditory/speech perception & processing [Chao et al., 2018, Arnal and Giraud, 2012, Gagnepain et al., 2012, Davis et al., 2011, Wild et al., 2010, Poeppel et al., 2008]. Our findings of dominant low-to-low and low-to-high frequency coupling top-down are consistent with these accounts, and could well serve to enhance the animal's engagement in the task [Lakatos et al., 2016, Park et al., 2015]. In addition, the top-down coupling signal we observed may also be carrying predictive information, being consistent with frequency ranges which have been shown to carry prediction-update

eNeuro Accepted Manuscript

signals [Chao et al., 2018]. We cannot dissociate between attentive or predictive signals here, however.

We found PAC and AAC to offer similar accounts of information processing. This could be due to a high degree of shared informational content between the two measures; it remains unclear how these measures differ, and how AAC could function mechanistically in the brain. To the degree that PAC and AAC offer complementary, non-overlapping information, it is possible that top-down influences are exerted more broadly through various CFC types including both PAC and AAC, and others such as phase synchronization [Fries, 2005].

We observed the same pattern of results in synthetic stimuli. The overall lower coupling strength we observed in synthetic stimuli could be a consequence of the coding differences that were previously observed between synthetic and intact stimuli [Fukushima et al., 2014], or they could be driving these coding differences. Lower coupling strength in synthetic stimuli could also be a result of the modulatory effect of attention being lower for synthetic compared to natural stimuli, perhaps because animals pay less attention to unnatural, ecologically irrelevant stimuli. The observation of higher coupling strength in spectrally rich (SPS) over spectrally poor (EPS) stimuli, envelope-intact stimuli suggests enhanced encoding and processing of information-rich stimuli. This is also consistent witho our previous results which showed that information about spectrally rich stimuli was better maintained than information about spectrally flat stimuli, at least across the first two sectors (S1,S2) of the auditory hierarchy. In the highest-order auditory sector (S4), decoding performance showed differences across a broader frequency range among VOC and EPS than among VOC and SPS.

The fact that we find the same coupling patterns across natural and synthetic stimuli points to the existence of conserved cross-frequency signatures of bottom-up and top-down information processing in auditory cortex. These findings have important implications for theories of neural processing such as predictive coding. In theoretical implementations of predictive coding, the presence of nonlinearities in going from predictions to prediction errors may induce cross-frequency interactions in the top-down direction. These should be less prevalent if not absent in the bottom-up direction as prediction errors are thought to accumulate linearly. Our finding of predominant low frequency to *lowγ* cross-frequency coupling bottom-up suggests nonlinearities may also play a role in bottom-up processing, allowing the modulation of γ power in higher-order areas by the phase of low frequency rhythms in lower order areas, for example. Overall though, our finding of widespread predominant cross-frequency interactions in the top-down direction is in agreement with the predictive coding framework.

Many of the theoretical propositions for spectral asymmetries in forward and backwards message passing in predictive coding do not consider the role of attention, however. In predictive coding, attention is mediated by optimising the precision of ascending prediction errors in a context-sensitive fashion. Physiologically, this corresponds to changing the gain of lower levels (usually considered to involve fast spiking inhibitory interneurons and some form of coherence or synchronous gain). Crucially, the effect of attention adds an extra level of

eNeuro Accepted Manuscript

nonlinearity that could be mediated by backward connections, and, implicitly, cross frequency coupling.

We employed a method based on the canonical correlation framework that allowed us to estimate directed cross-frequency coupling strength in a computationally efficient framework. Many previous studies and methods to estimate cross-frequency coupling do not obtain directional estimates [Cohen, 2008, Canolty et al., 2006, Bruns and Eckhorn, 2004, Tort et al., 2010, Voytek et al., 2013, van Wijk et al., 2015], and thus do not allow for feedfoward and feedback components to be teased apart. Studies that do take direction into account [Bastos et al., 2012, Michalareas et al., 2016, Bastos et al., 2015, Fontolan et al., 2014] employ separate measures to look at coupling strength (e.g. through coherence) and directional information flow (e.g. through Granger causality), and do not take *cross*-frequency interactions into account. The dynamic causal modelling (DCM) framework [Friston et al., 2017, Friston et al., 2003, Chen et al., 2008] does allow for the computation of directed coupling across frequencies [Furl et al., 2014]. Practically however, to enhance computational efficiency, current implementations of DCM reduce the dimensionality of the data by applying a singular value decomposition to the data from the source region X, and then projecting Y into this reduced space to compute coupling estimates [Chen et al., 2008]. The variance preserving dimensions in the source and target space are not necessarily the dimensions that maximize correlations between source and target space, in which case interactions may be missed. In contrast, the canonical correlation framework employed here has the advantage of finding low dimensional representations which maximize coupling between the source (X) and target (Y) data. A similar approach has been used to obtain estimates of cross-frequency interactions in MEG data [Sato et al., 2010], however without the directional Granger-causal component included here.

In summary, we revealed distinct cross-frequency signatures of top-down and bottom-up information processing. These signatures are largely preserved across coupling types and stimulus types, suggesting they are a general hallmark of information processing in auditory cortex. Our finding of prominent low-to-high frequency coupling top-down extends the current view of low-to-high frequency interactions in auditory cortex, which primarily emphasized their involvement in bottom-up processes. We employed a method that allows for the computationally efficient estimation of directed cross-frequency interactions. Altogether, this extends our understanding of how information is propagated up and down the cortical hierarchy, with significant implications for theories of neural information processing such predictive coding.

References

Arnal and Giraud, 2012. Arnal, L. H. and Giraud, A.-L. (2012). Cortical oscillations and sensory predictions. *Trends in Cognitive Sciences*, 16(7):390–398.

eNeuro Accepted Manuscript

Aru et al., 2015. Aru, J., Aru, J., Priesemann, V., Wibral, M., Lana, L., Pipa, G., Singer, W., and Vicente, R. (2015). Untangling cross-frequency coupling in neuroscience. *Current Opinion in Neurobiology*, 31:51–61.

Bastos et al., 2012. Bastos, A. M., Usrey, W. M., Adams, R. A., Mangun, G. R., Fries, P., and Friston, K. J. (2012). Canonical Microcircuits for Predictive Coding. *Neuron*, 76(4):695–711.

Bastos et al., 2015. Bastos, A. M., Vezoli, J., Bosman, C. A., Schoffelen, J.-M., Oostenveld, R., Dowdall, J. R., De Weerd, P., Kennedy, H., and Fries, P. (2015). Visual Areas Exert Feedforward and Feedback Influences through Distinct Frequency Channels. *Neuron*, 85(2):390–401.

Bosman et al., 2012. Bosman, C. A., Schoffelen, J.-M., Brunet, N., Oostenveld, R., Bastos, A. M., Womelsdorf, T., Rubehn, B., Stieglitz, T., De Weerd, P., and Fries, P. (2012). Attentional Stimulus Selection through Selective Synchronization between Monkey Visual Areas. *Neuron*, 75(5):875–888.

Bressler and Richter, 2015. Bressler, S. L. and Richter, C. G. (2015). ScienceDirect Interareal oscillatory synchronization in top-down neocortical processing. *Current Opinion in Neurobiology*, 31:62–66.

Bruns and Eckhorn, 2004. Bruns, A. and Eckhorn, R. (2004). Task-related coupling from high- to low-frequency signals among visual cortical areas in human subdural recordings. *International Journal of Psychophysiology*, 51(2):97–116.

Buzsáki et al., 2012. Buzsáki, G., Anastassiou, C. A., and Koch, C. (2012). The origin of extracellular fields and currents — EEG, ECoG, LFP and spikes. *Nature Reviews Neuroscience*, 13(6):1–14.

Canolty et al., 2006. Canolty, R. T., Edwards, E., Dalal, S. S., Soltani, M., Nagarajan, S. S., Kirsch, H. E., Berger, M. S., Barbaro, N. M., and Knight, R. T. (2006). High Gamma Power Is Phase-Locked to Theta Oscillations in Human Neocortex. *Science*, 313(5793):1626–1628.

Canolty and Knight, 2010. Canolty, R. T. and Knight, R. T. (2010). The functional role of cross-frequency coupling. *Trends in Cognitive Sciences*, 14(11):506–515.

Chao et al., 2018. Chao, Z. C., Takaura, K., Wang, L., Fujii, N., and Dehaene, S. (2018). Large-Scale Cortical Networks for Hierarchical Prediction and Prediction Error in the Primate Brain. *Neuron*, pages 1–30.

Chen et al., 2008. Chen, C. C., Kiebel, S. J., and Friston, K. J. (2008). Dynamic causal modelling of induced responses. *NeuroImage*, 41(4):1293–1312.

Cohen, 2008. Cohen, M. X. (2008). Assessing transient cross-frequency coupling in EEG data. *Journal of Neuroscience Methods*, 168(2):494–499.

eNeuro Accepted Manuscript

Colgin, 2015. Colgin, L. L. (2015). Theta–gamma coupling in the entorhinal–hippocampal system. *Current Opinion in Neurobiology*, 31:45–50.

Davis et al., 2011. Davis, M. H., Ford, M. A., Kherif, F., and Johnsrude, I. S. (2011). Does Semantic Context Benefit Speech Understanding through. *Journal of Cognitive Neuroscience*, pages 1–21.

Doesburg et al., 2012. Doesburg, S. M., Green, J. J., McDonald, J. J., and Ward, L. M. (2012). Theta modulation of inter-regional gamma synchronization during auditory attention control. *Brain Research*, 1431(C):77–85.

Durstewitz, 2017. Durstewitz, D. (2017). Advanced Data Analysis in Neuroscience. *Springer International Publishing*.

Fontolan et al., 2014. Fontolan, L., Morillon, B., Liegeois-Chauvel, C., and Giraud, A.-L. (2014). The contribution of frequency-specific activity to hierarchical information processing in the human auditory cortex. *Nature Communications*, 5(1):1–10.

Fries, 2005. Fries, P. (2005). A mechanism for cognitive dynamics: neuronal communication through neuronal coherence. *Trends in Cognitive Sciences*, 9(10):474–480.

Friston, 2008. Friston, K. (2008). Hierarchical Models in the Brain. *PLOS Computational Biology*, 4(11):e1000211–24.

Friston et al., 2003. Friston, K. J., Harrison, L., and Penny, W. (2003). Dynamic causal modelling. *NeuroImage*, 19(4):1273–1302.

Friston et al., 2017. Friston, K. J., Preller, K. H., Mathys, C., Cagnan, H., Heinzle, J., Razi, A., and Zeidman, P. (2017). Dynamic causal modelling revisited. *NeuroImage*, pages 1–0.

Fukushima et al., 2012. Fukushima, M., Saunders, R. C., Leopold, D. A., Mishkin, M., and Averbeck, B. B. (2012). Spontaneous high-gamma band activity reflects functional organization of auditory cortex in the awake macaque. *Neuron*, 74(5):899–910.

Fukushima et al., 2014. Fukushima, M., Saunders, R. C., Leopold, D. A., Mishkin, M., and Averbeck, B. B. (2014). Differential Coding of Conspecific Vocalizations in the Ventral Auditory Cortical Stream. *Journal of Neuroscience*, 34(13):4665–4676.

eNeuro Accepted Manuscript

Furl et al., 2014. Furl, N., Coppola, R., Averbeck, B. B., and Weinberger, D. R. (2014). Cross-Frequency Power Coupling Between Hierarchically Organized Face-Selective Areas. *Cerebral cortex (New York, N.Y. : 1991)*, 24(9):2409–2420.

Gagnepain et al., 2012. Gagnepain, P., Henson, R. N., and Davis, M. H. (2012). Temporal Predictive Codes for Spoken Words in Auditory Cortex. *Current Biology*, 22(7):615–621.

Giraud and Poeppel, 2012. Giraud, A.-L. and Poeppel, D. (2012). Cortical oscillations and speech processing: emerging computational principles and operations. *Nature Neuroscience*, 15(4):511–517.

Hyafil et al., 2015a. Hyafil, A., Fontolan, L., Kabdebon, C., Gutkin, B., and Giraud, A.-L. (2015a). Speech encoding by coupled cortical theta and gamma oscillations. *eLife*, 4:3958.

Hyafil et al., 2015b. Hyafil, A., Giraud, A.-L., Fontolan, L., and Gutkin, B. (2015b). Neural Cross-Frequency Coupling: Connecting Architectures, Mechanisms, and Functions. *Trends in Neurosciences*, 38(11):725–740.

Jensen and Colgin, 2007. Jensen, O. and Colgin, L. L. (2007). Cross-frequency coupling between neuronal oscillations. *Trends in Cognitive Sciences*, 11(7):267–269.

Jirsa and Mueller, 2013. Jirsa, V. and Mueller, V. (2013). Cross-frequency coupling in real and virtual brain networks. *Frontiers in Computational Neuroscience*, pages 1–25.

Kellis et al., 2010. Kellis, S., Miller, K., Thomson, K., Brown, R., House, P., and Greger, B. (2010). Decoding spoken words using local field potentials recorded from the cortical surface. *Journal of Neural Engineering*, 7(5):056007–20.

Kendrick et al., 2011. Kendrick, K. M., Zhan, Y., Fischer, H., Nicol, A. U., Zhang, X., and Feng, J. (2011). Learning alters theta amplitude, theta-gamma coupling and neuronal synchronization in inferotemporal cortex. *BMC Neuroscience*, 12(1):55.

Kikuchi et al., 2010. Kikuchi, Y., Horwitz, B., and Mishkin, M. (2010). Hierarchical auditory processing directed rostrally along the monkey's supratemporal plane. *The Journal of neuroscience : the official journal of the Society for Neuroscience*, 30(39):13021–13030.

Kveraga et al., 2007. Kveraga, K., Ghuman, A. S., and Bar, M. (2007). Top-down predictions in the cognitive brain. *Brain and Cognition*, 65(2):145–168.

eNeuro Accepted Manuscript

Lakatos et al., 2016. Lakatos, P., Barczak, A., Neymotin, S. A., McGinnis, T., Ross, D., Javitt, D. C., and O'Connell, M. N. (2016). Global dynamics of selective attention and its lapses in primary auditory cortex. *Nature Neuroscience*, 19(12):1707–1717.

Lakatos et al., 2008. Lakatos, P., Karmos, G., Mehta, A. D., Ulbert, I., and Schroeder, C. E. (2008). Entrainment of Neuronal Oscillations as a Mechanism of Attentional Selection. *Science*, 320(5872):110–113.

Landau and Fries, 2012. Landau, A. N. and Fries, P. (2012). Attention Samples Stimuli Rhythmically. *Current Biology*, 22(11):1000–1004.

Lee et al., 2013. Lee, J. H., Whittington, M. A., and Kopell, N. J. (2013). Top-Down Beta Rhythms Support Selective Attention via Interlaminar Interaction: A Model. *PLOS Computational Biology*, 9(8):e1003164–23.

Maris and Oostenveld, 2007. Maris, E. and Oostenveld, R. (2007). Nonparametric statistical testing of EEG- and MEG-data. *Journal of Neuroscience Methods*, 164(1):177–190.

Michalareas et al., 2016. Michalareas, G., Vezoli, J., van Pelt, S., Schoffelen, J.-M., Kennedy, H., and Fries, P. (2016). Alpha-Beta and Gamma Rhythms Subserve Feedback and Feedforward Influences among Human Visual Cortical Areas. *Neuron*, 89(2):384–397.

Nichols and Holmes, 2001. Nichols, T. E. and Holmes, A. P. (2001). Nonparametric Permutation Tests For Functional Neuroimaging: A Primer with Examples. *Human Brain Mapping*, 15:1–25.

Park et al., 2015. Park, H., Ince, R. A. A., Schyns, P. G., Thut, G., and Gross, J. (2015). Frontal Top-Down Signals Increase Coupling of Auditory Low-Frequency Oscillations to Continuous Speech in Human Listeners. *CURBIO*, 25(12):1649–1653.

Poeppel et al., 2008. Poeppel, D., Idsardi, W. J., and van Wassenhove, V. (2008). Speech perception at the interface of neurobiology and linguistics. *Philosophical Transactions of the Royal Society B: Biological Sciences*, 363(1493):1071–1086.

Ray and Maunsell, 2011. Ray, S. and Maunsell, J. H. R. (2011). Different Origins of Gamma Rhythm and High-Gamma Activity in Macaque Visual Cortex. *PLoS Biology*, 9(4):e1000610–15.

Richter et al., 2017. Richter, C. G., Thompson, W. H., Bosman, C. A., and Fries, P. (2017). Top-Down Beta Enhances Bottom-Up Gamma. *Journal of Neuroscience*, 37(28):6698–6711.

eNeuro Accepted Manuscript

Romanski and Averbeck, 2009. Romanski, L. M. and Averbeck, B. B. (2009). The Primate Cortical Auditory System and Neural Representation of Conspecific Vocalizations. *Annual Review of Neuroscience*, 32(1):315–346.

Salin and Bullier, 1995. Salin, P.-A. and Bullier, J. (1995). Corticocortical Connections in the Visual System: Structure and Function. *Physiological Review*, 75(1):1–48.

Sato et al., 2010. Sato, J. R., Fujita, A., Cardoso, E. F., Thomaz, C. E., Brammer, M. J., and Amaro Jr, E. (2010). Analyzing the connectivity between regions of interest: An approach based on cluster Granger causality for fMRI data analysis. *NeuroImage*, 52(4):1444–1455.

Schack et al., 2002. Schack, B., Vath, N., Petsche, H., Geissler, H. G., and Moeller, E. (2002). Phase-coupling of theta-gamma EEG rhythms during short-term memory processing. *International Journal of Psychophysiology*, 44:143–163.

Schroeder et al., 2010. Schroeder, C. E., Wilson, D. A., Radman, T., Scharfman, H., and Lakatos, P. (2010). Dynamics of Active Sensing and perceptual selection. *Current Opinion in Neurobiology*, 20(2):172–176.

Scott et al., 2015. Scott, B. H., Leccese, P. A., Saleem, K. S., Kikuchi, Y., Mullarkey, M. P., Fukushima, M., Mishkin, M., and Saunders, R. C. (2015). Intrinsic Connections of the Core Auditory Cortical Regions and Rostral Supratemporal Plane in the Macaque Monkey. *Cerebral cortex (New York, N.Y. : 1991)*, 7:bhv277–32.

Tort et al., 2010. Tort, A. B. L., Komorowski, R., Eichenbaum, H., and Kopell, N. (2010). Measuring Phase-Amplitude Coupling Between Neuronal Oscillations of Different Frequencies. *Journal of Neurophysiology*, 104(2):1195–1210.

Tort et al., 2009. Tort, A. B. L., Komorowski, R. W., Manns, J. R., Kopell, N. J., and Eichenbaum, H. (2009). Theta–gamma coupling increases during the learning of item– context associations. *PNAS*, 106(49):20942–20947.

Tort et al., 2008. Tort, A. B. L., Kramer, M. A., Thorn, C., Gibson, D. J., Kubota, Y., Graybriel, A. M., and Kopell, N. J. (2008). Dynamic cross-frequency couplings of local field potential oscillations in rat striatum and hippocampus during performance of a T-maze task. *PNAS*, 105(51):20517–20522.

van Wijk et al., 2015. van Wijk, B. C. M., Jha, A., Penny, W., and Litvak, V. (2015). Parametric estimation of cross-frequency coupling. *Journal of Neuroscience Methods*, 243:94–102.

eNeuro Accepted Manuscript

Voytek et al., 2013. Voytek, B., D'Esposito, M., Crone, N., and Knight, R. T. (2013). A method for event-related phase/amplitude coupling. *NeuroImage*, 64(C):416–424.

Wild et al., 2010. Wild, C. J., Davis, M. H., and Johnsrude, I. S. (2010). Human auditory cortex is sensitive to the perceived clarity of speech. *NeuroImage*, 60(2):1–13.

Wild et al., 2012. Wild, C. J., Yusuf, A., Wilson, D. E., Peelle, J. E., Davis, M. H., and Johnsrude, I. S. (2012). Effortful Listening: The Processing of Degraded Speech Depends Critically on Attention. *Journal of Neuroscience*, 32(40):14010–14021.